Identification Method for Single-line-to-ground Faults with Line Break Based on Phasor Measurement in Distribution Networks

Yadong Liu, Zichang Li, Yingjie Yan, Guanghui He, *Member*, *IEEE*, Jian Fang, Kejun Li, and Xiuchen Jiang

***Abstract*—The single-line-to-ground faults with line breaks (SLGFs-LBs) occur more and more frequently in distribution networks and can cause major safety accidents. It is difficult to distinguish the single-line-to-ground faults (SLGFs) in resonant grounding systems and ungrounding systems due to the same electrical characteristics on the source side and uncertain operation conditions of distribution networks. This paper proposes a method for distinguishing SLGFs-LBs and SLGFs. First, the source-side and load-side voltage characteristics of SLGFs and SLGFs-LBs are analyzed, and the phase difference between the voltages of the fault phase and non-fault phase on the load side is selected as the identification criterion. Phasor measurement units (PMUs) are selected as measuring devices. Then, the effects of operation conditions and external devices in distribution networks on the proposed method are discussed, and the phase errors caused by them are calculated to correct the identification method. Finally, the field testing and simulation experiments are conducted to verify the effectiveness and robustness of the proposed method.**

***Index Terms*—Distribution network, phase measurement unit, single-line-to-ground fault (SLGF), identification method, influencing factor.**

I. Introduction

FAULTS in distribution networks are the root cause of more than 80% of outages in power systems [1]. Therefore, small-current grounding systems, including resonant grounding systems and ungrounding systems, are widely used in medium-voltage distribution networks around the world, since they can keep running for a few hours after single-line-to-ground faults (SLGFs), which account for 80% of total number of faults in distribution networks [2]. However, due to meteorological disasters, overloading wires, and mechanical disruptions [3], single-line-to-ground faults with line breaks (SLGFs-LBs) occur more and more frequently in recent years. SLGFs-LBs exhibit the same voltage and current characteristics as SLGFs before the fault point, so it is difficult to distinguish them at substations. SLGFs-LBs can go undetected for hours in small-current grounding systems but the consequences caused by SLGFs-LBs such as overvoltages [4] and step voltages [5] are serious. Moreover, the resulting fires and electric shocks could cause injuries and even deaths. Therefore, the effective SLGF-LB identification is the key of reducing its threat to lives and property of people.

Researchers have already paid much attention to various short-circuit faults and made many achievements [2], [5], [6]. However, due to the unobvious fault characteristics and lack of relevant experience on SLGF-LB in the actual operation of distribution networks, few studies have been conducted on the SLGF-LB identification and there is no relay protection device for SLGFs-LBs in distribution networks [7]. In recent years, with the increasing frequency of SLGFs-LBs and development of distribution automation systems, SLGFs-LBs have gradually aroused the attention of researchers. So far, two kinds of identification method for SLGFs-LBs have been proposed. One is based on the combination of electrical parameters, which could be calculated by theoretical derivation at different locations in the distribution network. For example, in [3], the source-side sequence currents are used as the criterion to locate and identify the fault lines and the source-side and load-side three-phase voltage amplitudes are selected to detect SLGFs-LBs. References [7] and [8] take the amplitudes and phases of three-phase currents before and after a fault as the main criterion to detect SLGFs-LBs, and the amplitudes of three-phase voltages are taken as an auxiliary criterion to identify whether the fault is grounded or not and the location of grounding point. Reference [9] studies the electrical characteristics of negative-sequence current, zero-sequence current, and the three-phase voltages on the load side when SLGFs-LBs occur based on the actual operation data of distribution networks. The other one is to process monitored electrical data through big data technology or machine learning methods. Reference [10] extracts the voltage and current characteristics on the primary side of distribution

Manuscript received: May 11, 2021; revised: September 17, 2021; accepted: January 2, 2022. Date of CrossCheck: January 2, 2022. Date of online publication: April 11, 2022.

This work was supported in part by National Science Foundation of China (No. 51707117).

Y. Liu (corresponding author), Z. Li, Y. Yan, G. He, K. Li, and X. Jiang are with Institute of Intelligent Power Transmission and Distribution. Shanghai Jiao Tong University, Shanghai 201100, China (e-mail: lyd@sjtu. edu. cn; lzc940872816@sjtu. edu. cn; yanyingjie@sjtu. edu. cn; heguanghui@sjtu. edu. cn; fjenglish@163.com; 397455963@qq.com).

J. Fang is with the Electric Power Test Institute of Guangzhou Power Supply Bureau Co., Ltd., Guangzhou 510420, China (e-mail: XCjiang@sjtu.edu.cn).

DOI: 10.35833/MPCE.2021.000288

transformers after SLGFs-LBs occur on the medium-voltage side in the distribution networks and the association-rule algorithm is selected as the identification method. However, due to the limitation of application scenarios and incomplete development, big data technology or machine learning methods has not been widely used in the distribution network.

The aforementioned detection methods for SLGFs-LBs select a variety of electrical parameters at different locations as the identification criteria for SLGFs-LBs, and have certain reference values. However, the robustness of these identification methods could be reduced by influencing factors in practical distribution networks [11], [12]. For example, the practical distribution networks do not operate under ideal conditions because problems such as network imbalance and frequency fluctuation are common. In addition, with the development of distribution networks, load types and their switching become more and more frequent, which will lead to the frequent and severe fluctuations of three-phase currents and power factor in distribution networks. Some of them can even inject high-order voltage and current harmonics into distribution networks.

In short, a simple, effective, and robust identification method should be proposed to distinguish SLGFs-LBs and SLGFs. Firstly, the suitable parameters should be selected as the identification criteria. The fundamental reason for the high concealment of SLGFs-LBs is that the electrical characteristics of SLGFs-LBs are almost the same as those of SLGFs on the source side, which makes it difficult to distinguish SLGFs and SLGFs-LBs. Therefore, the load-side electrical parameters could be considered as the identification criteria. Since the power system frequency monitoring network (FNET) was proposed in 2005 [13], the construction of wide area measurement system (WAMS) based on advanced local-area measurements that can realize synchronized measurement has made great progresses around the world [13], [14]. So far, the advanced local-area measurements such as phasor measurement units (PMUs) have recently been introduced as an efficient and powerful tool for real-time monitoring of different locations of distribution networks [15]. PMUs have entered the field of distribution network automation, and will definitely serve more application scenarios in the future [16]-[18]. In addition, considering the huge cost of installing PMUs at each bus or each side of lines in distribution networks [19], the branch PMU, which has multiple channels and can monitor several branch lines at the same time [20], could be installed at the intersection of multiple branch lines and selected as the measuring device to save costs. This paper proposes a criterion to distinguish SLGFs-LBs and SLGFs based on characteristics of the load-side three-phase voltages in distribution networks. The phase angle between the fault phase voltage and the vector sum of non-fault phase voltages on the load side is used as the criteria for the identification method, since PMU could realize high-resolution measurement of the phase angle of voltage [21]. The factors affecting the accuracy of the proposed criterion such as operation conditions and external devices are considered to improve the robustness of the proposed identification method.

The rest of this paper is organized as follows. Section II calculates the source-side and load-side three-phase voltages of SLGFs and SLGFs-LBs and analyzes their characteristics. The identification method for SLGFs-LBs based on load-side three-phase voltages is proposed and its influencing factors are listed and calculated in Section III. Section IV consists of simulation and field testing experiments, and the results verify the effectiveness and robustness of the proposed identification method. Section V concludes this paper.

II. Voltage Characteristics of SLGFs and SLGFs-LBs

Since the radial distribution networks are the most widely used around the world [22], the analysis in this paper is based on the distribution network powered by a single source. The equivalent circuits of SLGF and SLGF-LB are shown in Fig. 1(a) and (b), respectively. The SLGF and SLGF-LB are both single-line faults, but they are different at fault point F. The fault line of the SLGF is grounded through a resistance R_0 at F. However, the fault line of the SLGF-LB is broken at F and grounded through resistances R_1 and R_2. In Fig. 1, C is the three-phase grounding capacitances; O is the zero-potential point; N is the neutral point; E_A, E_B, and E_C are the three-phase voltages; and L is the inductance of the arc suppression coil for resonant grounding systems, in particular, L is ∞ for ungrounding systems.

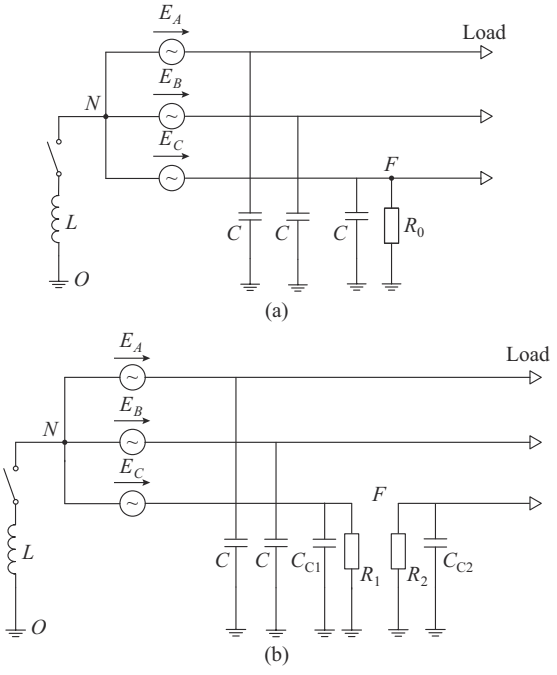

Fig. 1. Equivalent circuits of SLGF and SLGF-LB. (a) SLGF. (b) SLGF-LB.

A. Voltage Characteristics of SLGFs

Figure 1(a) illustrates the equivalent circuit of an SLGF, where the far-right node is connected to the load and phase C is grounded through resistance R_0. Assuming that v is the compensation degree of distribution networks, the relationship between the voltage of neutral point U_{Ng} and E_C is cal-

culated as:

$$\frac{E_C}{U_{Ng}} = -1 - \mathrm{j}R_0 B_C v \tag{1}$$

where $B_C = 3\omega C$ represents the three-phase susceptance of the distribution lines. To avoid the resonance during a fault, the power system is overcompensated [2], i. e., $v < 0$. The term $-1 - \mathrm{j}R_0 B_C v$ has a negative real part and a negative imaginary part due to the overcompensation. Thus, E_C is ahead of U_{Ng} by 90°-180°.

The vector diagram of SLGFs is shown as Fig. 2. We take the three-phase voltages E_A, E_B, and E_C as the references. Thus, the neutral point N is fixed and the location of the zero-potential point O is associated with the grounding resistance R_0. When R_0 increases from 0 to ∞, the zero-potential point O moves from M to N through a semicircle, and the trajectory of the zero-potential point O is located at the left side of MN. Note that, for SLGFs, the source-side three-phase voltages to the grounding points U_{Ag}, U_{Bg}, and U_{Cg} are equal to the load-side three-phase voltages due to direct connection of distribution lines.

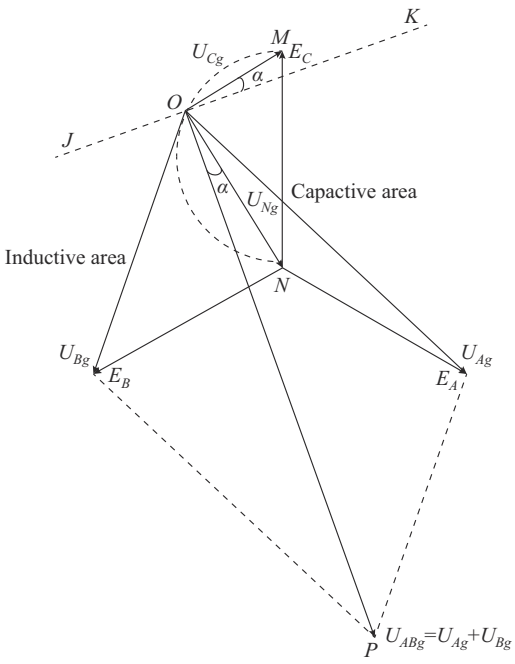

Fig. 2. Vector diagram of SLGFs.

We denote θ as the phase difference between the fault phase voltage and the vector sum of non-fault phase voltages on the load side. Through the online data processing function of PMUs, θ could be directly obtained. The value of θ depends on the symmetry of the three-phase voltage angles, instead of amplitudes. Therefore, the type of distribution network does not affect the measurement result of θ. Besides, since the PMUs are installed on the load side of each distribution line, the line faults will be reflected on the measurement value of θ, regardless of the location of faults. We assume that $\theta < 0$ means the fault phase voltage is ahead of the vector sum of non-fault phase voltages. Therefore, θ has a value of [−180°, 180°].

As shown in Fig. 2, for SLGFs, the fault phase voltage and the sum of non-fault phase voltages on the load side are U_{Cg} and $U_{ABg} = U_{Ag} + U_{Bg}$, respectively. It can be observed that the phase difference between U_{Cg} and U_{ABg} is $\theta = \angle MOP = 90° + \alpha$, where α is the angle between U_{Cg} and line JK, and JK is the auxiliary line perpendicular to U_{ABg}. Since R_0 and α are greater than 0, we have $\theta = 90° + \alpha > 90°$. Consequently, $|\theta|$ is larger than 90° for SLGFs. From Fig. 2, it is concluded that α will increase from 0° to 90° as zero-potential point O moves from M to N.

B. Voltage Characteristics of SLGFs-LBs

Unlike SLGFs, a distribution line break due to a SLGF-LB might bring different voltage characteristics on the source and load sides. As shown in Fig. 1(b), the grounding resistances on the source and load sides are R_1 and R_2, respectively; the grounding capacitances of fault phase on the source and load sides are C_{C1} and C_{C2}, respectively; and the grounding capacitance of non-fault phases is C. The relationship between the voltage of neutral point U_{Nb} and E_C during an SLGF-LB is calculated as:

$$\frac{E_C}{U_{Nb}} = -1 - \mathrm{j}R_1 B_C v \tag{2}$$

where $B_C = 2\omega C + \omega C_{C1}$.

Based on (2), considering the overcompensation in distribution networks, the vector diagram of the SLGF-LB on the load side is shown in Fig. 3; where U_{Ab}, U_{Bb}, and U_{Cb} are the load-side voltages of phases A, B, and C, respectively.

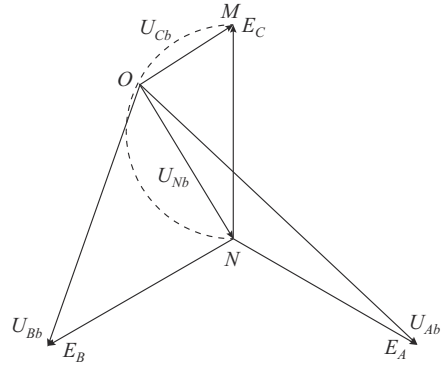

Fig. 3. Vector diagram of SLGFs-LBs.

As can be observed from Figs. 2 and 3, the voltage vector diagrams of SLGFs and SLGFs-LBs on the source side are similar, so it is difficult to distinguish the voltage characteristics on the source side.

However, the load-side voltages could be considered for fault differentiation. Considering two types of loads, in a balanced three-phase power system, we consider $Z_A = Z_B = Z_C = Z_1$ for Y-type load and $Z_{AB} = Z_{AC} = Z_{BC} = Z_2$ for △-type load. In Fig. 1(b), the branches of C and C_{C2} can be regarded as open circuit because the impedances of C and C_{C2} are generally 5 pF/m for overhead lines and 250 pF/m for cables [23]-[25], which are much larger than the grounding resistance R_2. The equivalent load impedance Z_k is relevant to load type, where $Z_k = 2Z_1$ for Y-type load and $Z_k = (2/3)Z_2$ for △-type load.

The equivalent load impedance Z_k consists of resistance R_k, inductance L_k, and capacitance C_k. Hence, U_{Cbl} is used to distinguish the load-side voltage of phase C, which can be expressed through a simplified model, as shown in Fig. 4. The simplified load-side model is an RLC circuit formed by three elements, i.e., R_k+R_2, L_k, and C_k.

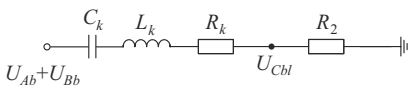

Fig. 4. Simplified load-side model of SLGF-LB.

According to Fig. 4, U_{Cbl} can be calculated as:

$$U_{Cbl}=\frac{R_2(U_{Ab}+U_{Bb})}{\sqrt{\left(2\pi fL_k-\frac{1}{2\pi fC_k}\right)^2+(R_2+R_k)^2}\,(\cos\theta+\mathrm{j}\sin\theta)} \tag{3}$$

Figure 5 shows the load-side phase relationship of SLGFs-LBs, where U_{ABb} is the vector sum of U_{Ab} and U_{Bb}. When the system load is inductive, $\theta<0$ and U_{Cbl} lies in the inductive region; and when the system load is capacitive, $\theta>0$ and U_{Cbl} lies in the capacitive region.

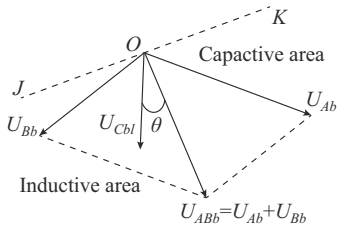

Fig. 5. Load-side phase relationship of SLGFs-LBs.

Referring to (4), $|\theta|$ has a range of (0°, 90°) for a SLGF-LB, and $|\theta|$ decreases as the grounding resistance R_2 increases.

$$\theta=\arctan\left(\frac{\frac{1}{2\pi fC_k}-2\pi fL_k}{R_2+R_k}\right) \tag{4}$$

According to (4), $|\theta|$ is smaller than 90° for SLGFs-LBs. Compared with the conclusion in Section II-A, different ranges of $|\theta|$ can be used as the criterion to distinguish SLGFs-LBs and SLGFs, and the identification criteria are summarized as: ① when $|\theta|$ has a range of $[\theta_1, 180°]$, an SLGF occurs; ② when $|\theta|$ has a range of $[0°, \theta_2]$, an SLGF-LB occurs. Theoretically, $\theta_1=\theta_2=90°$. However, considering the limitation of practical ranges of grounding resistance, overcompensation degree, and parameters of distribution lines in actual distribution networks, the values of θ_1 and θ_2 are different from the theoretical values according to (1) and (4), and the value of $|\theta|$ is determined by the ratio of network parameters.

According to the survey on resistivity ranges of different urban grounding media, the minimum grounding resistances of SLGFs and SLGFs-LBs can be calculated as 180 Ω according to the grounding model of distribution line [6]. Table I presents the typical properties of distribution lines and overcompensation degree in 10 kV radial distribution networks. In order to reserve some margin, $R_{\min}=125\,\Omega$ is selected as the critical point of the minimum grounding resistance. When $R_{\min}=125\,\Omega$, $|\theta|$ for SLGFs and SLGFs-LBs can be calculated as 93.02° and 86.12° by (1) and (4), respectively. Note that, according to (4), only the load-side grounding resistance R_2 should be considered in the above calculation process of $|\theta|$ for SLGFs-LBs; therefore, $\theta_1=$ 93.02°, and $\theta_2=86.12°$. And θ_1 and θ_2 deviate farther from each other as $R_{\min}$ increases. According to the design limitation of relay protection devices, the identification method mentioned above may fail when the value of grounding resistance approaches the critical point.

TABLE I
TYPICAL PROPERTIES OF DISTRIBUTION LINES AND OVERCOMPENSATION DEGREE

Capacitance (pF/m)	Length (km)	Overcompensation degree (%)	Load current (A)
(5, 250)	(6, 20)	(–10, 0)	(5, 630)

III. INFLUENCING FACTORS FOR IDENTIFICATION METHOD

The practical distribution networks vary in structures and operation environments, which contain many factors that may affect the power flow of distribution networks. Therefore, the accuracy of the proposed identification method might be influenced by them. According to their properties, the influencing factors can be divided into two categories, i.e., operation conditions and external devices.

A. Effect of Operation Conditions

The operation conditions consist of network imbalance, power frequency fluctuation, and voltage harmonic distortion. The analyses of their causes and influence on the proposed identification method are shown as follows.

1) Network Imbalance

Due to unbalanced loads and line parameters during the normal operation, the network imbalance is a common phenomenon in distribution networks. The network voltage imbalance should be less than 4% [26], i.e., $U_N\%=4\%$. Considering the extreme case in which $U_N\%=4\%$, the maximum non-fault voltage of phase B is $(1+U_N\%)U_{Bb}$. Referring to Fig. 6, the angle between U_{ABb} and U'_{ABb} is the error caused by voltage imbalance.

For the non-fault phases, there is no difference between the source-side and load-side voltages. Thus, the vector diagrams of phases without SLGF and SLGF-LB are similar. The maximum phases error $\Delta\theta_{\max}$ caused by the voltage imbalance can be calculated as 2.02° from Fig. 6 according to analytic geometry theory.

2) Power Frequency Fluctuation

When the load power is not equal to the generated power, there will be changes in the speed of the generator rotor. Thus, the power frequency of distribution networks will fluctuate. The maximum allowable deviation of power frequency should not exceed 1 Hz [27]. And the maximum phase error $\Delta\theta_{\max}$ could be calculated as 0.3° in the extreme case [27].

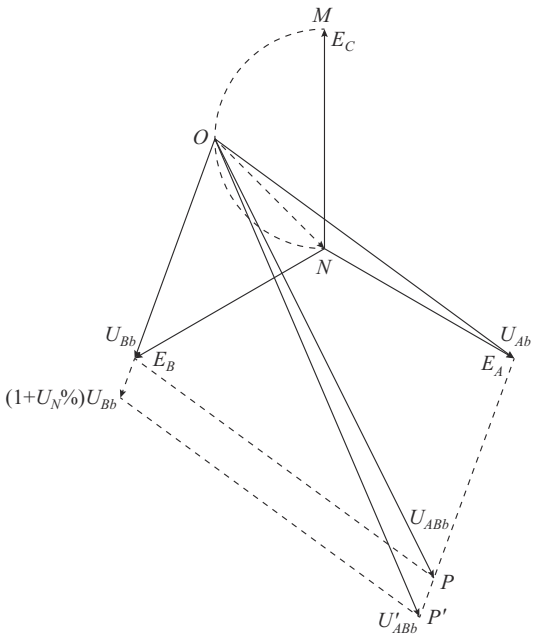

Fig. 6. Error caused by network imbalance.

3) Voltage Harmonic Distortion

Power supply equipment with non-linear impedance is common in distribution networks, which will inject harmonic voltages into distribution networks and cause the voltage harmonic distortion. At the medium-voltage side of distribution networks, the rate of voltage harmonic distortion is limited to less than 4% [28]. Similar to the network imbalance, the maximum phase error $\Delta\theta_{\max}$ caused by voltage harmonic distortion can be calculated as 2.02°.

B. Effect of External Devices

With the development of the power system, more and more external devices have been installed in distribution networks such as three-phase loads, distributed energy resources (DERs), and measuring devices. Their influences on the proposed identification method are analyzed as follows.

1) Power Factor

In the power grid, most of the reactive power is generated by induction motors and power transformers without reactive power compensation measures, and the reactive load produced by them in the power grid may reach 80% of the total network load [29]. In order to reserve some margin, 90% is set as the critical point of reactive power proportion. The power factor is calculated as 0.436 when the reactive load accounts for 90% of the total network load. According to (1) and (2), the ratio of reactive load has no influence on the source-side and load-side three-phase voltages for SLGFs; while only the load-side voltages for SLGFs-LBs are affected by power factor. It can be observed from (3) and (4) that as the ratio of reactive load increases, the power factor decreases and $|\theta|$ shows an increasing trend. Therefore, the error caused by power factor only affects the threshold of $|\theta|$ for SLGFs-LBs, i.e., θ_2. Ignoring other influencing factors, according to (4), the maximum value of $|\theta|$ for the SLGF-LBs can be calculated as 83.66° by means of trigonometric function; while $|\theta|$ for the SLGF varies from 90° to 180°. Therefore, the errors caused by power factor can be calculated as −6.34° for SLGFs-LBs and 0° for SLGFs, i.e., −6.34° for θ_2 and 0° for θ_1, respectively.

2) DER Access

With the development of renewable energy technology, a considerable number of DERs have been connected to distribution networks [22]. When an SLGF or SLGF-LB occurs in the distribution network, according to Figs. 2 and 3, there will be undervoltage and overvoltage in the faulty phase, which is downstream of the faulty point. During this period, DERs will automatically switch to one of the following three operation states.

1) If the detection result is that the undervoltage and overvoltage are caused by a fault, the DERs will cease to energize and trip immediately [30].

2) If DERs cannot detect the fault, they will regard the undervoltage and overvoltage as temporary voltage disturbances in distribution networks. When one of three-phase voltages do not fluctuate within the range of the applicable voltage, i.e., [0.5 p.u.,1.2 p.u.] [30], DERs should cease to energize and trip immediately.

3) If DERs cannot detect the fault and the three-phase voltages fluctuate within the range of the applicable voltage, DERs shall operate at low-voltage ride-through or high-voltage ride-through state [30]. However, there are time limits for DER operation with such voltage disturbances. The longest duration of DER operation with overvoltage and undervoltage is 12 s and 20 s, respectively, which is related to the capacity and design of DERs [30]. Since SLGFs and SLGFs-LBs mentioned in this paper are permanent faults, the duration of overvoltage and undervoltage caused by them will exceed the time limit, and DERs will cease to energize and trip.

In summary, DERs will cease to energize and trip at last when SLGFs or SLGFs-LBs occur. Since the proposed identification criteria is based on the phase of steady-state voltages on the load side, DER access has no influence on the proposed identification method for SLGFs-LBs.

3) Measuring Devices

PMUs are selected as the measuring devices in this paper due to the synchronized measurement, widespread application, and low cost. Therefore, according to the design and application specifications of PMUs, the maximum phase error $\Delta\theta_{\max}$ caused by PMUs is 0.5° when monitoring the phase difference of three-phase voltages [31].

C. Recommended Value

According to the analysis of the causes of various factors, different kinds of errors depend on different properties of components in distribution networks. Therefore, these factors above are independent, which means that extreme conditions for each factor can exist simultaneously. It can be concluded from the calculation process in Section II that the criterion is based on calculations of trigonometric functions such as arctangent function in (4), and the angle error is small compared with the criterion threshold. Therefore, within the limit, phase errors $\Delta\theta$ caused by operation conditions and exter-

nal devices can be summed to obtain θ_1 and θ_2. According to the analysis in Section III-A and III-B, the errors caused by operation conditions and external devices are summarized in Table II. These errors will result in the expansion of the intervals of θ for distinguishing SLGFs and SLGFs-LBs, which may lead to the overlap of the two criterion intervals. Therefore, the critical errors should be selected according to the maximum expansion criterion intervals. As shown in Table II, the factors other than power factor will affect SLGFs and SLGFs-LBs in different ways.

TABLE II
PROPERTIES OF FACTORS AFFECTING θ_1 AND θ_2

Factor	Condition	$\Delta\theta$ for SLGF (°)	$\Delta\theta$ for SLGF-LB (°)	$\Delta\theta_{1,\max}$ (°)	$\Delta\theta_{2,\max}$ (°)
Voltage imbalance	(−4%, 4%]	(−2.02, 2.02]	(−2.02, 2.02]	−2.02	2.02
Frequency fluctuation	(−1 Hz, 1 Hz]	(−0.3, 0.3]	(−0.3, 0.3]	−0.30	0.30
Voltage harmonic distortion	(−4%, 4%]	(−2.02, 2.02]	(−2.02, 2.02]	−2.02	2.02
Power factor	The maximum reactive power load is not larger than 90%	0	(−90, −6.34)	0	−6.34
DER access	Cease to energize and trip				
Measuring device		(−0.5, 0.5]	(−0.5, 0.5]	−0.50	0.50

θ_1 and θ_2 can be calculated through summing up phase errors. Therefore, errors for θ_1 and θ_2 are calculated as −4.84° and −1.5°, respectively. Referring to Table II, the rounding calculation results of θ_1 and θ_2 are 88° and 86°, respectively. The margins of the selected thresholds are 0.18° for θ_1 and 0.52° for θ_2, respectively, which indicate that the thresholds of residuals between actual values and theoretical calculation values of θ_1 and θ_2 for SLGFs and SLGF-LBs under the combined influence of multiple influencing factors. According to the analysis above, the identification method can be corrected as: ① when $|\theta|$ has a range of [89°, 180°], an SLGF occurs; ② when $|\theta|$ has a range of [0°, 86°], an SLGF-LB occurs.

Considering the longest duration of low-voltage ride-through for DERs, $|\theta|$, which is measured with a duration of at least 20 s after the fault occurs, can be used for distinguishing SLGFs-LBs and SLGFs. Compared with the allowable running time (1-2 hours) of SLGFs in small-current grounding systems, the duration of 20 s is short. Therefore, the proposed method can effectively reduce the running time of SLGFs-LBs.

IV. EXPERIMENTAL AND SIMULATION RESULTS

To verify the effectiveness and robustness of the proposed identification method for SLGFs-LBs, field experiments and simulation experiments are conducted in this paper. Field experiments focus on the validation of theoretical results in Section II, while simulation experiments aim to verify the robustness of the proposed identification method.

A. Experimental Environment and Results

Field experiments are conducted at a real-world testing base in Henan, China. The topological structure of the testing power system is shown in Fig. 7. The rated voltage is 10 kV and the power frequency is 50 Hz. For outgoing lines L1, L2, L3, and L4, three-phase capacitors C_1, C_2, C_3, and C_4 are installed as capacitive loads, respectively, and C_1 = 2 μF, $C_2 = C_3 = 4$ μF, and $C_4 = 0.8$ μF. At L7, the neutral point could be ungrounded or resonant grounded with a −7.7% compensation degree. Considering the limitations of experimental equipment and the safe operation of the experimental distribution system, the influencing factors are not included in field experiments. Therefore, the purpose of field experiments is to verify the adaptability of the identification method in Section II to different topologies and parameters of distribution networks, i.e., different grounding methods, grounding points, and grounding resistances.

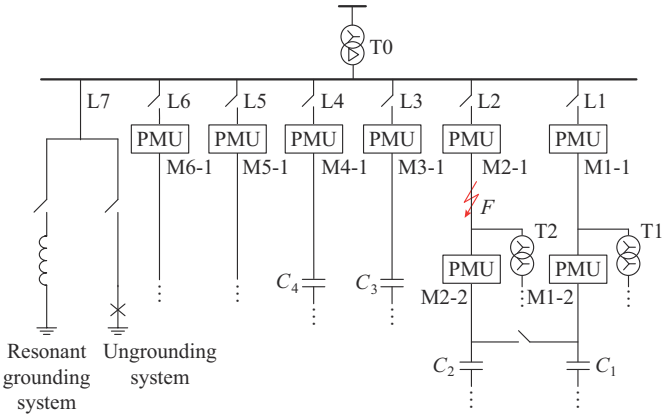

Fig. 7. Topological structure of testing power system.

The PMU used in this experiment is designed by Shanghai Jiao Tong University (SJTU), China. Typical parameters of each PMU are illustrated in Table III.

TABLE III
TYPICAL PARAMETERS OF PMUS DESIGNED BY SJTU

Sampling frequency (kHz)	Voltage measurement range (kV)	Current measurement range (A)	Measurement accuracy (%)	Running current (A)	Clock synchronization mode
[1, 4]	[0, 30]	[0, 600]	≤0.5	[5, 600]	GPS/ Beidou

The power supply mode of these PMUs is inductive energy acquisition plus lithium battery [32]. One PMU is equipped at the beginning of each outgoing line. The data

collected by the PMUs are transmitted through wireless communication (4G in this case) to the workstation. The data are used for fault identification and the crew is notified of the results. For L1 and L2, a PMU is required on the load side. Since the proposed identification criteria is three-phase steady-state voltage, the accuracy of measurement is not affected by the sampling frequency if the sampling rate satisfies Nyquist sampling theory. According to the engineering practical experience [31] and rated parameters of the chosen PMUs [32], the sampling rate of the PMUs is set to be 4 kHz. The fault point F is located on L2. Both the source-side and load-side grounding resistances are adjustable through the resistance cabinet. The three-phase load is purely capacitive. Figure 8 shows the schematic diagram of fault generator.

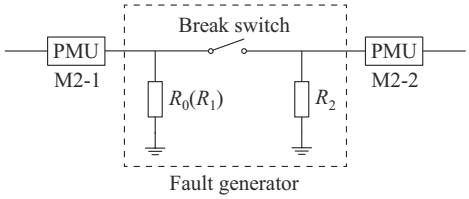

Fig. 8. Schematic diagram of fault generator.

The results of field experiments are illustrated in Fig. 9. The grounding resistances are set as the independent variables from 125 Ω to 5000 Ω. Figure 9(a) and (b) shows experimental results of $|\theta|$ in ungrounding systems, including SLGFs, source-side grounding SLGFs-LBs, and load-side grounding SLGFs-LBs; while Fig. 9(c) and (d) shows experimental results of $|\theta|$ in resonant grounding systems. Their specific meanings are annotated in Fig. 9. According to Fig. 9, $|\theta|$ is within the range of [0°, 86.12°] and [93.02°, 180°] for SLGFs and SLGFs-LBs, respectively, regardless of topologies and parameters of distribution networks, which verifies the effectiveness of the proposed method in Section II.

According to Fig. 9(a) and (c), as the grounding resistance increases, $|\theta|$ increases for SLGFs and decreases for load-side grounding SLGFs-LBs, which is not affected by neutral point grounding methods. Therefore, the proposed identification method is more sensitive to high-impedance faults. However, as shown in Fig. 9(b) and (d), the change of $|\theta|$ for source-side grounding SLGFs-LBs is irregular as the source-side grounding resistance increases. In addition, $|\theta|$ for source-side grounding SLGFs-LBs is within the range of [0°, 0.3°] in both ungrounding systems and resonant grounding systems, which could be equivalent to load-side grounding high-impedance SLGFs-LBs, consistent with theoretical calculation results in Section II. In addition, by comparing Fig. 9(a) with (c) and Fig. 9(b) with (d), it can be concluded that, as the grounding resistance increases, $|\theta|$ in resonant grounding systems changes more smoothly than that in ungrounding systems for all faults, since the connection of the arc suppression coil could reduce the fault current, which will delay the change of $|\theta|$.

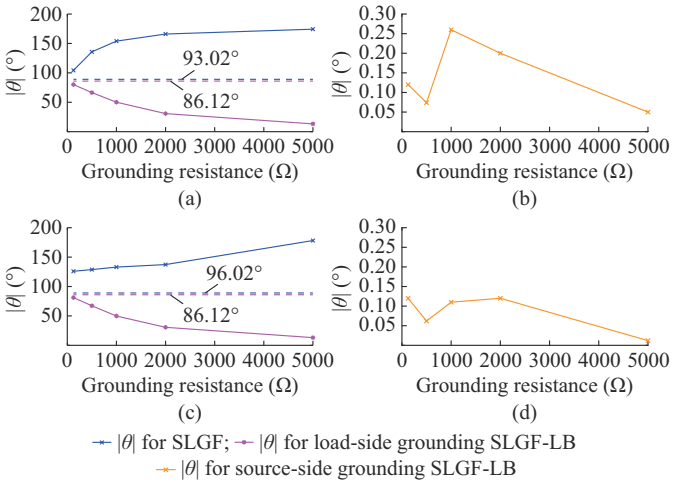

Fig. 9. Results of field experiments. (a) Load-side grounding SLGF-LB and SLGF in ungrounded system. (b) Source-side grounding SLGF-LB in ungrounded system. (c) Load-side grounding SLGF-LB and SLGF in resonant grounding system. (d) Source-side grounding SLGF-LB in resonant grounding system.

B. Simulation Model and Results

To verify the robustness of the proposed identification method for SLGFs-LBs, a 10 kV IEEE standard 10-node model built with PSCAD/EMTDC simulation software is shown in Fig. 10.

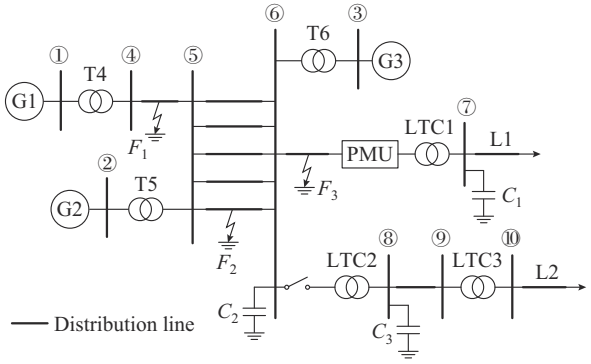

Fig. 10. Diagram of 10 kV IEEE standard 10-node simulation model.

There are three generators (G1, G2, and G3) in this simulation model. The main transformers (T4, T5, and T6) and distribution transformers (LTC1, LTC2, and LTC3) both use star-triangle windings, the ratios of which are 110 kV/10.5 kV and 10 kV/0.38 kV, respectively. The type of distribution lines could be selected from either overhead line or cable; and π model is selected as the equivalent circuit model, whose properties are presented in Table IV. The whole distribution system is resonant grounding and the overcompensation degree is set to be −10%. Three single-line faults are set at the beginning, middle, and end of distribution lines in the simulation model, i.e., F_1, F_2, and F_3, respectively, to simulate the influence of fault locations. The PMU is installed at the entrance of the primary side of LTC1. The whole simulation lasts for 2 s. Among them, the frequency-dependent model is selected as the transmission model of overhead lines and cables, and the power frequency is set to be 50 Hz.

TABLE IV
PROPERTIES OF SIMULATION MODEL OF OVERHEAD LINE OR CABLE

Distribution line	Property	Resistance (Ω/km)	Inductive reactance (Ω/km)	Capacitive reactance (MΩ·km)
Overhead line	Positive impedance	0.18	3.14	0.20
	Zero impedance	0.23	10.40	0.41
Cable	Positive impedance	0.22	0.76	0.21
	Zero impedance	2.24	3.02	0.32

Simulation experiments are carried out to analyze $|\theta|$ for SLGFs and SLGFs-LBs, which occur at different locations of the distribution network composed of different distribution lines. Besides, the effects of power factor, network imbalance (±4%), frequency fluctuation (±1 Hz), and voltage harmonic distortion (±4%) on the value of $|\theta|$ are also simulated. In simulation experiments, load-side grounding resistance is set as the independent variable from 125 Ω to 5000 Ω; while other network parameters such as the overcompensation degree and length of distribution lines are set as the critical value presented in Table I, which is −10% and 20 km, respectively.

The simulation results for different fault locations and types of distribution lines are shown in Fig. 11.

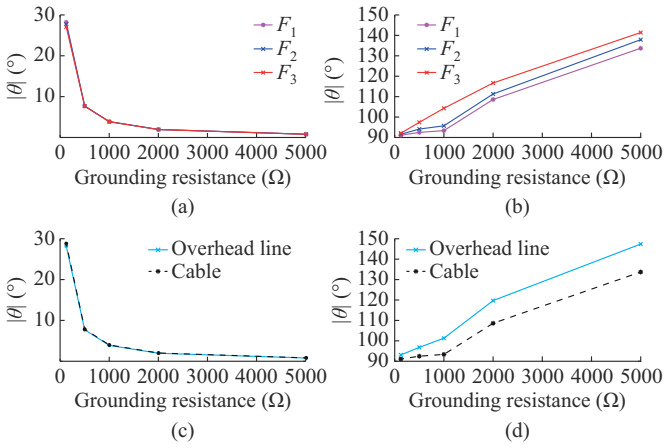

Fig. 11. Simulation results for different fault locations and types of distribution lines. (a) $|\theta|$ at different fault locations for SLGF-LB. (b) $|\theta|$ at different fault locations for SLGF. (c) $|\theta|$ on different distribution lines for SLGF-LB. (d) $|\theta|$ on different distribution lines for SLGF.

Figure 11(a) and (b) shows the simulation results of $|\theta|$ for overhead line when single-line faults occur at different locations of distribution networks. It can be concluded from Fig. 11(a) and (b) that the location of fault does not affect the trend of $|\theta|$ as the grounding resistance increases, while the value of $|\theta|$ varies with the change of the distance between the fault location and PMU. As the distance grows, the value of $|\theta|$ gets closer to the threshold values, namely 86° for SLGFs-LBs and 89° for SLGFs, respectively, since fault characteristics are less obvious as the fault gets farther away from the monitoring point. In addition, since parallel lines have the same voltage, when the fault occurs at F_2, according to Fig. 10, $|\theta|$ measured from the PMU will not be influenced by other branch lines.

Figure 11(c) and (d) shows the simulation results of $|\theta|$ on overhead lines and cables for SLGF-LB and SLGF, repectively. The fault location is set at F_1 in Fig. 10 to make $|\theta|$ closer to the threshold values. According to Fig. 11(c) and (d), the types of distribution lines do not influence the trend of $|\theta|$ as the grounding resistance increases. However, the value of $|\theta|$ is related to the type of distribution lines. When the cable is selected, the value of $|\theta|$ is closer to threshold values because the capacitance of cable is greater than that of overhead line, which is reflected by B_C of (1) and (2). It could be calculated that the value of $|\theta|$ tends to approach 90° as B_C increases, regardless of faults types, which is consistent with simulation results in Fig. 11(c) and (d).

The simulation results of influencing factors are illustrated in Fig. 12. According to the simulation results shown in Fig. 11, the fault location is set at F_1, and the overhead line is selected to make the value of $|\theta|$ closer to the threshold values. Considering that the maximum error caused by PMUs is limited [32], it can be added directly to the results of $|\theta|$. Therefore, the simulation experiments for measuring devices are not conducted.

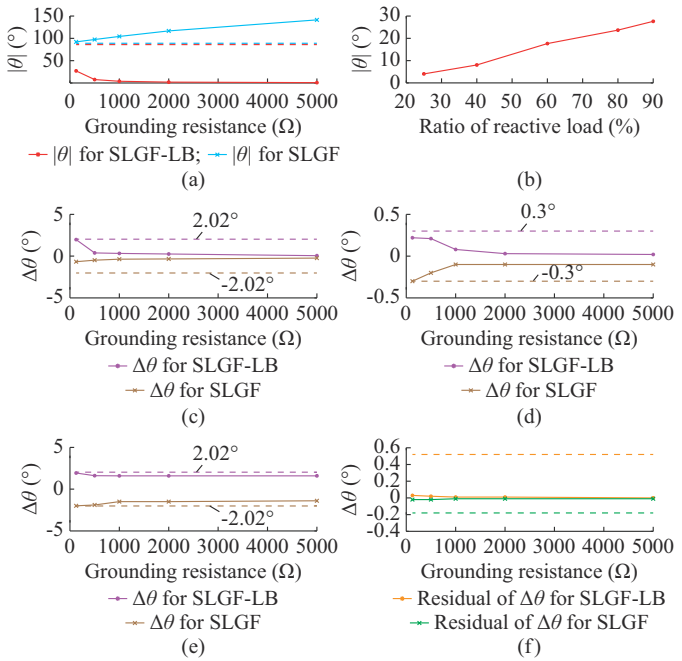

Fig. 12. Simulation results of θ and $\Delta\theta$ under different influences influencing factors. (a) $|\theta|$. (b) Influence of power factor. (c) Influence of network imbalance. (d) Influence of frequency fluctuation. (e) Influence of voltage harmonic distortion. (f) Residual analysis.

Figure 12(a) shows the simulation results of the relationship between $|\theta|$ and load-side grounding resistance, regardless of errors caused by operation conditions and external devices. The ratio of reactive load is set to be 90%. It can be observed from Fig. 12(a) that the range of $|\theta|$ is always within the limit of thresholds for SLGFs and SLGFs-LBs. In addition, as the load-side grounding resistance increases, $|\theta|$ in-

creases for SLGFs and decreases for SLGFs-LBs, consistent with Fig. 9(a) and (c), respectively.

Figure 12(b) shows the simulation results of the influence of power factor on $|\theta|$ for SLGFs-LBs, since power factor only affects $|\theta|$ for SLGFs-LBs. The load-side grounding resistance is set to be 125 Ω. The ratio of reactive load is set to be 90%, 80%, 60%, 40%, and 25%, respectively. It can be concluded that as the ratio of reactive load decreases, $|\theta|$ for SLGFs-LBs decreases. In addition, the simulation results of $|\theta|$ for SLGFs-LBs do not exceed 83.66°, consistent with theoretical results from (4) and Section III-C.

Figure 12(c)-(e) illustrates the effect of different influencing factors. The ratio of reactive load is set to be 90%. From Fig. 12(c)-(e), it can be concluded that $\Delta\theta$ caused by different influencing factors is always within the range of theoretical thresholds. For example, $|\Delta\theta|$ caused by network imbalance and voltage harmonic distortion does not exceed 2.02°; and the influence of frequency fluctuation on $|\theta|$ is always within the limit of ±0.3°. Moreover, the three factors mentioned above have the opposite impacts on $|\theta|$ for SLGFs-LBs and SLGFs. In addition, the influence of those factors on $|\theta|$ decreases as load-side grounding resistance increases. The basic reason is that the fault current also decreases as the load-side grounding resistance increases.

The residual analysis is selected to verify the superposition principle of different kinds of errors. The simulation experiment is conducted when the influencing factors reach the extreme conditions at the same time. Theoretical values indicate numerical sum of $\Delta\theta$ based on results from Fig. 12(b)-(e), while measured values represent the simulation sum of $\Delta\theta$ in this experiment. According to Fig. 12(f), even under extreme conditions, the residuals of $\Delta\theta$ for SLGFs and SLGFs-LBs are not beyond the margins. Therefore, the superposition principle is applicable based on simulation results.

In summary, the simulation results show that the ranges of $|\theta|$ and its errors are consistent with theoretical calculation results in Sections II and III. Therefore, the proposed identification method can keep high accuracy and robustness even in extreme cases based on simulation results.

V. Conclusion

In this paper, an identification method based on phase relationship between the fault phase voltage and the vector sum of non-fault phase voltages is proposed to distinguish SLGF-LBs and SLGFs in radial small-current grounding distribution networks. The conclusions can be drawn as follows.

1) The characteristics for source-side voltage of SLGFs and SLGFs-LBs are similar, which makes it difficult to distinguish them on the source side.

2) Due to the difference in electrical structures, the load-side voltages of SLGFs and SLGFs-LBs exhibit different characteristics. Therefore, the load-side voltages can be used as the criterion to distinguish SLGFs-LBs and SLGFs. The phase difference between the fault phase voltage and the vector sum of non-fault phase voltages on the load side, i.e., θ, is selected as the criteria. Without considering influencing factors, when $|\theta|$ has a range of [93.02°, 180°], SLGFs occur; and when $|\theta|$ has a range of [0°, 86.12°], SLGFs-LBs occur. Note that, the minimum grounding resistance could be calculated as $R_{\min} = 125\,\Omega$; and the identification method may become invalid when the value of grounding resistance is around $R_{\min}$.

3) To enhance the robustness of the proposed method, the errors resulting from operation conditions and external devices are calculated. After correction, the upper boundary of $|\theta|$ is 86° for SLGFs-LBs; while the lower boundary of $|\theta|$ is 89° for SLGFs.

References

[1] M. Gholami, A. Abbaspour, M. Moeini-Aghtaie *et al*., "Detecting the location of short-circuit faults in active distribution network using PMU-based state estimation," *IEEE Transactions on Smart Grid*, vol. 11, no. 2, pp. 1396-1406, Mar. 2020.

[2] Y. Du, Y. Liu, Q. Shao *et al.*, "Single line-to-ground faulted line detection of distribution systems with resonant grounding based on feature fusion framework," *IEEE Transactions on Power Delivery*, vol. 34, no. 4, pp. 1766-1775, Aug. 2019.

[3] Z. Li, Y. Liu, Y. Yan *et al.*, "An identification method for asymmetric faults with line breaks based on low-voltage side data in distribution networks," *IEEE Transactions on Power Delivery*, vol. 36, no. 6, pp. 3629-3639, Dec. 2021.

[4] A. Kalyuzhny, "Analysis of temporary overvoltages during open-phase faults in distribution networks with resonant grounding," *IEEE Transactions on Power Delivery*, vol. 30, no. 1, pp. 420-427, Feb. 2015.

[5] Z. Lv, B. Ning, W. Luo *et al.*, "A real time monitoring method for single-line break fault based on dual-terminal information of distribution network with fault tolerant," in *Proceedings of 2019 IEEE 3rd Conference on Energy Internet and Energy System Integration (EI2)*, Changsha, China, Nov. 2019, pp. 2587-2592.

[6] S. Zhang, T. Zang, W. Zhang *et al*., "Fault feeder identification in non-effectively grounded distribution network with secondary earth fault," *Journal of Modern Power Systems and Clean Energy*, vol. 9, no. 5, pp. 1137-1148, Sept. 2021.

[7] Q. Kang, W. Cong, M. Wang *et al.*, "Analyses and judgment methods of single-phase broken-line fault for loaded distribution line," in *Proceedings of 2016 IEEE PES Asia-Pacific Power and Energy Engineering Conference (APPEEC),* Xi'an, China, Oct. 2016, pp. 482-486.

[8] F. Shi and W. Cong, "Methodology to differentiate type of single-phase line break fault in 10 kV ungrounded distribution networks," in *Proceedings of 2014 IEEE PES Asia-Pacific Power and Energy Engineering Conference(APPEEC)*, Hong Kong, China, Dec. 2014, pp. 1-6.

[9] S. Mohajeryami, M. Doostan, and Z. Salami, "An analysis of open-phase fault in power generation station," in *Proceedings of 2016 North American PowerSymposium (NAPS)*, Denver, USA, Sept. 2016, pp. 1-6.

[10] S. Wu, Y. Zhang, and Y. Su, "The medium-voltage distribution network fault diagnosis based on data association analysis," in *Proceedings of 2017 International Conference on Green Energy and Applications (ICGEA)*, Singapore, Dec. 2017, pp. 57-63.

[11] Y. Zhang, J. Wang, and M. E. Khodayar, "Graph-based faulted line identification using micro-PMU data in distribution systems," *IEEE Transactions on Smart Grid*, vol. 11, no. 5, pp. 3982-3992, Sept. 2020.

[12] M. Pignati, L. Zanni, P. Romano *et al.*, "Fault detection and faulted line identification in active distribution networks using synchrophasors-based real-time state estimation," *IEEE Transactions on Power Delivery*, vol. 32, no. 1, pp. 381-392, Feb. 2017.

[13] Z. Zhong, C. Xu, B. J. Billian *et al.*, "Power system frequency monitoring network (FNET) implementation," *IEEE Transactions on Power Systems*, vol. 20, no. 4, pp. 1914-1921, Nov. 2005.

[14] Y. Yan, Y. Liu, J. Fang *et al.*, "Application status and development trends for intelligent perception of distribution network," *High Voltage*. doi: 10.1049/hve2.12159

[15] Y. Bansal and R. Sodhi, "PMUs enabled tellegen's theorem-based fault identification method for unbalanced active distribution network usingrtds," *IEEE Systems Journal*, vol. 14, no. 3, pp. 4567-4578, Sept. 2020.

[16] N. A. S. P. I. (2014 Oct.). PMUs and synchrophasor data flows in north America. [Online]. Available: http://www. https://www.smartgrid.gov/document/pmus_and_synchrophasor_data_flows_north_america.

[17] T. Bi, H. Liu, Q. Feng *et al.*, "Dynamic phasor model-based synchrophasor estimation algorithm for M-class PMU," *IEEE Transactions on Power Delivery*, vol. 30, no. 3, pp. 1162-1171, Jun. 2015.
[18] K. Chauhan and R. Sodhi, "Placement of distribution-level phasor measurements for topological observability and monitoring of active distribution networks," *IEEE Transactions on Instrumentation and Measurement*, vol. 69, no. 6, pp. 3451-3460, Jun. 2020.
[19] M. Gholami, A. Abbaspour, M. Moeini-Aghtaie *et al.*, "Detecting the location of short-circuit faults in active distribution network using PMU-based state estimation," *IEEE Transactions on Smart Grid*, vol. 11, no. 2, pp. 1396-1406, Mar. 2020.
[20] Z. Wu, X. Du, W. Gu *et al*., "Optimal PMU placement considering load loss and relaying in distribution networks," *IEEE Access*, vol. 6, pp. 33645-33653, May 2018.
[21] P. Li, H. Su, C. Wang *et al.*, "PMU-based estimation of voltage-to-power sensitivity for distribution networks considering the sparsity of Jacobian matrix," *IEEE Access*, vol. 6, pp. 31307-31316, May 2018.
[22] S. He, H. Gao, H. Tian *et al*., "A two-stage robust optimal allocation model of distributed generation considering capacity curve and real-time price based demand response," *Journal of Modern Power Systems and Clean Energy*, vol. 9, no. 1, pp. 114-127, Jan. 2021.
[23] *IEEE Guide for the Parameter Measurement of AC Transmission Lines*, IEEE Std 1870-2019, 2019.
[24] A. Bendjabeur, A. Kouadri, and S. Mekhilef, "Novel technique for transmission line parameters estimation using synchronized sampled data," *IET Generation, Transmission & Distribution*, vol. 14, no. 3, pp. 506-515, Feb. 2020.
[25] Y. Xiang, X. Han, L. Wang *et al.*, "Resonance characteristics and damping techniques of grid-connected converter with the distributed capacitance of transmission line," in *Proceedings of 2018 13th IEEE Conference on Industrial Electronics and Applications (ICIEA)*, Wuhan, China, May 2018, pp. 491-496.
[26] *IEC Standard Voltages*, IEC 60038:2002, 2002.
[27] *IEEE Recommended Practice for Monitoring Electric Power Quality*, IEEE Std 1159-2019, 2019.
[28] I*EEE Recommended Practice and Requirements for Harmonic Control in Electric Power Systems*, IEEE Std 519-2014, 2014.
[29] *IEEE Guide for Identifying and Improving Voltage Quality in Power Systems*, IEEE Std 1250-2018, 2018
[30] *IEEE Standard for Interconnection and Interoperability of Distributed Energy Resources with Associated Electric Power Systems Interfaces*, IEEE Std 1547-2018, 2018.
[31] *IEEE Guide for Synchronization, Calibration, Testing, and Installation of Phasor Measurement Units (PMUs) for Power System Protection and Control*, IEEE Std C37.242-2013, 2021.
[32] X. Wang, X. Xie, S. Zhang *et al.*, "Micro-PMU for distribution power lines," *CIRED-Open Access Proceedings Journal*, vol. 2017, no. 1, pp. 333-337, Jan. 2017.

Yadong Liu received the B.E. degree in electronic & information from China University of Geosciences, Wuhan, China, in 2004. He received the M.D and Ph.D degrees of electrical engineering from Shanghai Jiao Tong University (SJTU), Shanghai, China, in 2008 and 2012, respectively. Currently, he is an Associate Researcher in School of Electronic Information and Electrical Engineering at SJTU. His current research interests include fault location detection and intelligent diagnosis of power equipment.

Zichang Li received the B.E. degree in electrical engineering and automation from Shanghai Jiao Tong University (SJTU), Shanghai, China, in 2019. Now he is working towards his M.E. degree in high voltage and insulation engineering at SJTU. His current research interests include fault diagnosis and location in distribution network.

Yingjie Yan received the B.E. and Ph.D. degrees from Shanghai Jiao Tong University (SJTU), Shanghai, China, in 2011 and 2018, respectively. Now, he is working in the Department of Electrical Engineering, SJTU. His current research interests include electric power equipment online monitoring, big data methods for fault diagnosis, and condition evaluation of power equipment and transmission lines in distribution network.

Guanghui He received the B.S. degree from the University of Electronic Science and Technology of China, Chengdu, China, in 2002, and the Ph.D. degree from Tsinghua University, Beijing, China, in 2007, both in electronic engineering. He is current an Associate Professor with the Department of Micro/Nano Electronics, Shanghai Jiao Tong University (SJTU), Shanghai, China. His main research interests include high-performance electromagnetic transient simulation, energy efficient algorithms and circuits design for wireless communication and artificial intelligent systems.

Jian Fang is a Senior Engineer with the Guangzhou Power Supply Bureau Co., Ltd. Electric Power Test Institute, Guangzhou, China. His main research interests include distribution network operation management, distribution network technology supervision, and distribution network new technology promotion.

Kejun Li received the B.Sc. degree from Shanghai Jiao Tong University (SJTU), Shanghai, China, in 2016. Currently, he is pursuing the master degree in SJTU. His main research interests include fault identification and location in distribution network.

Xiuchen Jiang received the B.S. degree from Shanghai Jiao Tong University (SJTU), Shanghai, China, in 1987, the M.D. degree in electrical engineering from Tsinghua University, Beijing, China, in 1992, and the Ph.D. degree in electrical engineering from SJTU, in 2001. He is currently a Full Professor with SJTU, where he has been the Director of the Electrical Power Department since 2002. His main research interests include electrical measuring technology and electrical apparatus automation.